ANALYSIS OF POLES AND ZEROS FOR
TAPERED LINK DESIGNS

DOUGLAS L. GIRVIN
and
WAYNE J. BOOK

Georgia Institute of Technology, School of Mechanical Engineering
Atlanta, GA 30332-0405

ABSTRACT

This chapter analyzes the pole and zero locations of a linearly-tapered Euler-Bernoulli beam pinned at one end and free at the other end. Of particular interest is the location of zeros of the transfer function from torque applied at the pin to displacement of the free end. When tapered beams are used as the links of light-weight robots, the existence of nonminimum phase (right half plane) zeros complicates the robot control problem. Tapering the beam gives the robot designer an additional design parameter when establishing the flexible dynamics. The pole and zero locations are determined from a transfer matrix model which is the exact solution for a uniform beam. The approximate results for a tapered model result from segmentation of the beam into segments of different but constant cross sections. The relative position of poles and zeros varies significantly as the rate of taper changes, which will have consequences on feedback stability and noncausal effects in inverse dynamics.

1. Introduction

1.1 Problem Definition

As research for new applications for industrial robots proceeds, one major area of research is in robot flexibility. Traditionally, industrial robots are designed with stiff links, so the dynamics of the links can be assumed negligible in positioning the robot. In theory then as the robot moves, the links remain straight and do not bend. The tip position of the robot can be found geometrically from joint position at any given moment. In flexible robotics the links are no longer assumed to be rigid. As the robot moves, the links flex which can cause unwanted vibrations in the robot. These vibrations can cause error in positioning the tip of the robot.

Some of the applications motivating research in this field are assembly of space structures, inspection of large structures, and nuclear waste retrieval. When transporting things to outer space, weight is always a concern. Light-weight robots designed for space

applications will be flexible and must be controlled as such. Large structures like airplanes and submarines require careful inspection to insure detection of flaws. The inspections can be laborious and repetitive which is ideal work for a robot. The large workspace dictates the links be as light as possible resulting in flexible links. An emerging area of research is remote handling of nuclear waste. Existing nuclear waste storage facilities are no longer safe and the waste needs to be removed and restored in safer containers. The old containers are very large, while the access is usually quite small. Again, a light-weight slender robot with a large workspace is required. All of these applications are driving the research in the field of flexible robotics.

A common problem with flexible systems is how to control the system accurately to position the end-point. Rigid link robots are typically collocated systems; that is, the actuators and sensors are located at the same location (ie., a joint). With a flexible system this is not always the case. Most flexible systems are noncollocated. The system output (actuator torque) is generally located at the base of the system, while the output (tip position) is located at the end of the system. Noncollocated systems exhibit nonminimum phase behavior which results directly from the system zeros in the right-half of the s-plane (RHP zeros).

Controller design for collocated systems has been heavily researched and is well understood compared to controller design for noncollocated systems. In noncollocated systems, uncertainties from model inaccuracies and modal truncation present fundamental problems with system performance and stability[20]. The fundamental difference between collocated and noncollocated systems is the presence of RHP zeros. To advance controller design for noncollocated systems, research needs to be conducted into the factors that affect the location of these RHP zeros. This research targets the relationship between RHP zeros and structural design.

1.2   Review of Related Research

Although research on RHP zeros is limited, there has been some notable research done in the past. Some of the research deals directly with the problems presented by nonminimum phase systems, while other research examines different techniques to change the system characteristics from nonminimum phase to minimum phase.

In 1988, Nebot and Brubaker[15] experimented with a single-link flexible manipulator. The manipulator was constructed from thin plates connected by several bridges along their length. This provided flexibility in the horizontal plane, while maintaining stiffness in the vertical plane and torsional mode. They analytically determined the location of the first six zeros and determined three of them to be RHP zeros. They concluded these RHP zeros pose a formidable constraint in the controller design task.

In 1989, Spector and Flashner[21] investigated the sensitivity effects of structural models for noncollocated control systems. They considered a pinned-free beam with discrete end-point mass and inertia. They used transfer matrices to analyze the system. From the results they concluded the following. First, accurate dynamic modeling is critical in noncollocated

control design. Poor modeling can result in interchanging the pole/zero order which produces phase errors resulting in closed-loop instability. Second, accurate modeling of zero location near the system bandwidth is critical in modeling noncollocated systems. Third, zeros are more sensitive to perturbations in system parameters and boundary conditions than modal frequencies. They suggest more research attention be given to modeling system zeros in noncollocated systems.

In 1990, Spector and Flashner[20] again studied modeling and design implications pertinent to noncollocated control. A similar system was used, a pinned-free beam without end-point mass, only the system was analyzed using wave number plane theory. They also studied the effects of varying sensor/actuator separation distance. Most conclusions are identical to those drawn from the previous paper. In addition, they concluded all noncollocated systems are nonminimum phase above some finite frequency (the location of the lowest RHP zero dictates this frequency), and this frequency increases as sensor/actuator distance increases. Again they recommend more research into the modeling of zeros in noncollocated systems.

The physical interpretation of the zeros of flexible mechanical systems is more difficult than the system poles, which are the natural frequencies. Miu[14] explained the zeros of simple flexible systems as the natural frequencies of constrained subsystems of the overall system. For a single beam the real zeros, both positive and negative, are the poles of the constrained subsystem consisting of the beam between the sensor and actuator. The complex zeros are the natural frequencies (complex poles) of a constrained subsystem consisting of the beam segments outside the sensor and actuator. The special case of sensor and actuator collocation gives all complex zeros alternating between the poles. The special case of a torque actuator at one end of a beam in bending and position sensor at the other end of that beam gives all real zeros. Miu further explains the real zeros as arising from the ability of a beam in bending to store energy locally in nonpropogating waves.

Also in 1990, Park and Asada[16,17] investigated a minimum phase flexible arm with a torque actuation mechanism. Basically they used a cable mechanism to transfer the torque actuation point from the base to the tip of the arm. Since the sensor and actuator are located at the same point, the system is minimum phase. They concluded the inverse dynamics solution does not diverge because the RHP zeros are relocated to the LHP by the torque transmission mechanism. Also end-point feedback control can be stabilized for this system with simple a P-D controller. Unfortunately, implementation of the transmission device on multi-link systems could be difficult.

In 1991, Park, Asada, and Rai[1] expanded their previous work on a minimum phase flexible arm with a torque transmission device. In this research they integrate structure and control design using Finite Element Analysis (FEA) to design the shape of the arm while constraining pole and zero location. Essentially, they use the FEA program to generate a design that will increase the fundamental natural frequency and use the torque transmission device to eliminate the RHP zeros. A prototype of the new system had not been tested at

that point, and the main contribution was a method to evaluate nonuniform beams for design applications.

1.3   Proposed Method of Approach

The underlying issue in noncollocated control is how to deal with the RHP zeros in the control algorithm. A major step in solving the problem is understanding what design parameters can be used to change the location of these RHP zeros. This research targets the relationship between RHP zero location and structural design. Specifically, how do changes in the shape of the structure (link) affect the location of these zeros?

Traditionally links are designed with uniform properties along the length because analytic solutions to this problem exist. A link with variable cross-section cannot be solved analytically, but with aid of a computer a numerical approximation can be found. The key to an accurate numerical solution is a good model of the system.

2. Nonminimum Phase Systems

2.1 System Characteristics

As mentioned before, a system is considered nonminimum phase if there are system zeros or poles located in the right half of the complex plane. Figures 2.1a and 2.1b graphically express the difference between minimum phase and nonminimum phase systems.
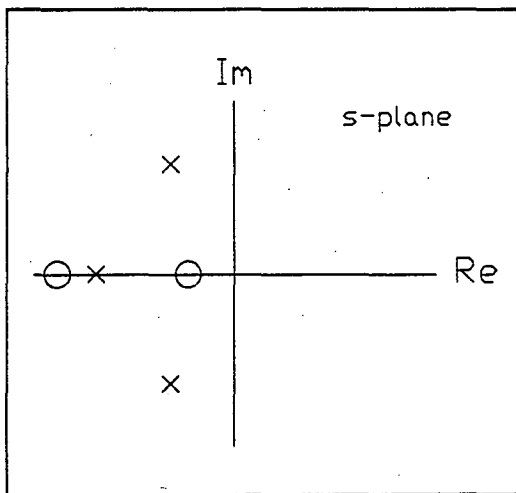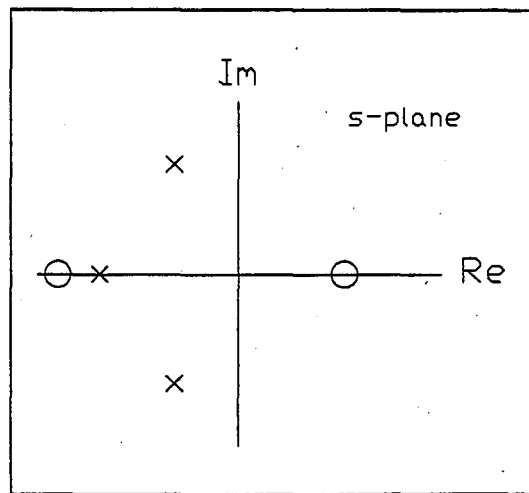

Figure 2.1a: Minimum Phase
Pole/Zero Pattern

Figure 2.1b: Nonminimum Phase
Pole/Zero Pattern

This is the case in the continuous-time domain. In the discrete-time domain (z-transform), the nonminimum phase zeros would lie outside the unit circle.

Often RHP zeros are called unstable zeros, but this is not good terminology. RHP zeros do not cause the plant to go unstable. Poles in the RHP will cause the system response to exponentially increase resulting in instability, but zeros do not cause this. It is the controller design that can cause the zeros to have an effect on system stability. For example, when using an inverse dynamics algorithm, the RHP zeros will become unstable poles in the inverse system. Now the controller has unstable poles which can cause the entire system to go unstable.

A noticeable characteristic of a nonminimum phase system is the time response to a step input. Figure 2.2 shows the difference between minimum phase (MP) and nonminimum phase (NMP) response of the tip position for a single-link flexible manipulator.
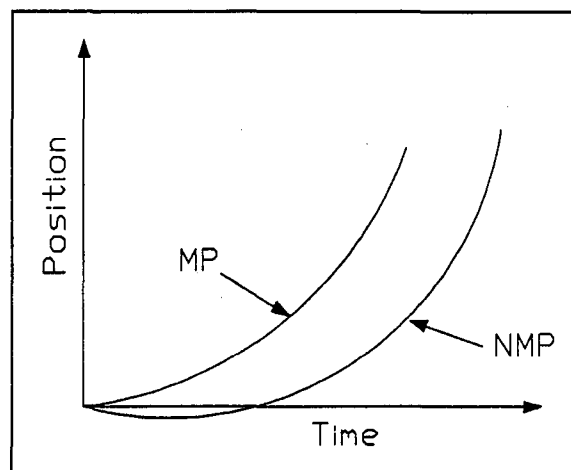

Figure 2.2: MP vs. NMP Time Response

Notice the tip of the NMP system initially starts to move in the direction opposite to the command. This type of response can be verified in Park and Asada's paper[16].

It has been stated that RHP zeros are indicative of a NMP system, but what physical phenomenon is responsible for NMP behavior? Miu[14] explains the zeros in terms of energy absorbed by a substructure of the flexible system. Real zeros result from absorption due to nonpropogating waves that can absorb energy through local mechanisms. Spector and Flashner[20] concluded that NMP behavior is an inescapable result of the finite wave propagation speed of elastic deformation in the structure. This wave propagation speed directly results in a time delay between system input and the corresponding system output. The time delay affects the system by reducing the phase margin. If the phase lag from the time delay exceeds the system phase margin (at the cutoff frequency), the system will be unstable.

These are some of the more prominent characteristics of nonminimum phase systems. Of interest in this research is the control of nonminimum phase systems and how to advance the research in this area. The following section describes some of the current techniques used to control nonminimum phase systems.

2.2 Control of Nonminimum Phase Systems

One method of controlling a nonminimum phase system studied by Misra[13] in 1989 is augmenting a nonminimum phase plant to make the overall system minimum phase. He used a "feedthrough" compensator so the augmented system was minimum phase. A feedthrough compensator was added so the poles of the compensated system move to the minimum phase zeros.

In 1987, Bayo[2] presented a structural finite element technique based on Bernoulli-Euler beam theory for open-loop control of flexible manipulators. The differential equations of motion are integrated in the frequency domain to determine the necessary torques for desired tip motion. The computed torque reproduced the desired trajectory without any overshoot, but closed-loop control was not investigated.

Another control algorithm investigated at Georgia Tech by Kwon and Book[5,9,10] used an inverse dynamic method to deal with a NMP flexible arm. The method is similar to Bayo's, only integration was carried out in the time domain. The dynamic equations of motion for a flexible manipulator can be written as:

$$\begin{bmatrix} M_{rr} & M_{rf} \\ M_{rf}^T & M_{ff} \end{bmatrix} \begin{Bmatrix} \ddot{q}_r \\ \ddot{q}_f \end{Bmatrix} + \begin{bmatrix} D_{rr} & D_{rf} \\ D_{rf}^T & D_{ff} \end{bmatrix} \begin{Bmatrix} \dot{q}_r \\ \dot{q}_f \end{Bmatrix} + \begin{bmatrix} 0 & 0 \\ 0 & K_{ff} \end{bmatrix} \begin{Bmatrix} q_r \\ q_f \end{Bmatrix} = \begin{bmatrix} B_r \\ B_f \end{bmatrix} \tau \qquad (2.1)$$

where,

q_r - Rigid body motion coordinate

q_f - Flexible motion coordinate

After some manipulation the inverse dynamics equations can be obtained in the following form:

$$\dot{X}_i = [A_i] X_i + [B_i] \dot{q}_{ir}$$
$$\tau = [C_i] X_i + [F_i] \dot{q}_{ir} \qquad (2.2)$$

where,

$$X_i = [q_f, q_f]^T \qquad q_{ir} = [q_r, q_r]^T$$

For the forward dynamic equations, the input is torque, and the outputs are all states. For the inverse dynamic system, the input is end-point desired trajectory, and the output is torque. The problem addressed is how to integrate these equations since the matrix $[A_i]$ has positive real poles. The RHP poles come from the RHP zeros in the original system. Their approach is to relax the solution range to include noncausal solutions allowing a unique stable solution of the inverse dynamic equations.

To better understand the inverse dynamics solution, some terminology needs to be defined. According to Kwon[9], a causal system is one in which the system output (impulse response) occurs after the system input (impulse). An anticausal system has the output (backward impulse response) before an input is applied. A noncausal system is a combination of both a causal system and a anticausal system.

To illustrate these concepts Figure 2.3 shows the motion of a flexible arm moving from point A to point B.
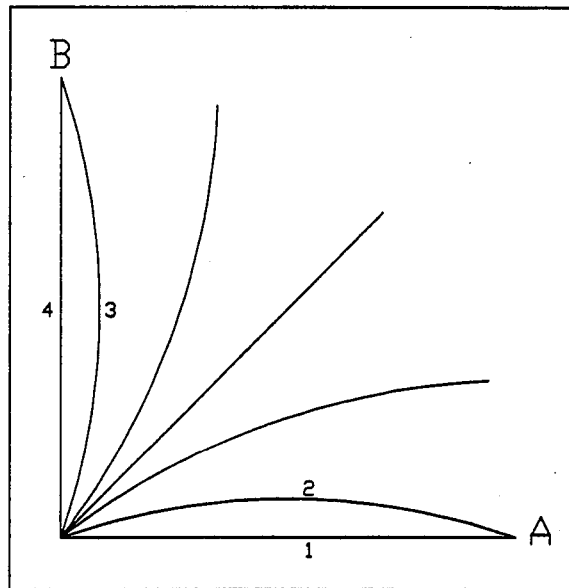

Figure 2.3: Flexible Link Motion

The two areas of interest on this curve are the start of motion and the end of motion. Motion starts as the arm moves from position 1 to 2, but the end-point does not move. The torque provided is applied to preshape the beam. This is the anticausal part of the inverse solution. The torque (output of the inverse system) occurs before the end-point (input to the inverse system) moves. When motion stops, the arm moves from position 3 to 4, again the end-point does not move. This represents the causal part of the inverse solution. The tip has stopped moving, but the torque continues to be applied. The torque applied between positions 4 and 5 is used to release the stored energy in the arm.

Since the motion can be divided into causal and anticausal parts, the solution to Eq. 2.2 can be divided into both causal and anticausal parts. Of interest to this research is the anticausal solution. The poles of the anticausal system are unstable and a direct result of the RHP zeros from the forward dynamic system. The ability to place these RHP zeros would be equivalent to placing the poles of the inverse anticausal problem. This would give the designer some freedom in choosing the location of the anticausal poles, and allow the system to be designed for specific needs. One benefit could be minimizing the time of

preshaping and the amount of energy provided by the actuator to preshape the beam before tip motion begins.

3. Transfer Matrix Method

3.1 Transfer Matrix Theory

Transfer matrices describe the interaction between two serially connected elements. These elements can be beams, springs, rotary joints, or many others. In 1979 Book, Majette, and Ma[6] and Book[4] (1974) used transfer matrices to develop an analysis package for flexible manipulators. They used transfer matrices to serially connect different types of elements to model the desired manipulator. Of interest in this paper is how to connect similar types of transfer matrices (beam elements) to model a beam with different cross-sectional area. Pestel and Leckie[18] provide an in depth discussion of transfer matrix derivations and applications.

Transfer matrices can be mathematically expressed by Eq. 3.1. The state vector u_i is given by the state vector u_{i-1} multiplied by the transfer matrix B.

$$u_i = [B_i]u_{i-1}$$

(3.1)

When elements are connected serially, the states at the interface of two elements must be equal. By ordered multiplication of the transfer matrices, intermediate states can be eliminated to determine the transfer matrix for the overall system.

The concept of state vector in transfer matrix theory is not to be confused with the state space form of modern control theory. The state equation in modern control theory relates the states of the system as a function of time. In transfer matrix theory the state equation relates the states as a function of position. The independent variable in transfer matrix theory is frequency, not time. The elements of the matrix B depend on the system driving frequency; therefore, the states will change as the system frequency changes. The transfer matrix B essentially contains the transformed dynamic equations of motion that govern the element in analytic form. Therefore, analytical solution of the transfer matrix alone does not involve numerical approximations. This is desirable since numerical approximations introduce error into the solution.

3.2 Modeling of a Nonuniform Beam

A single-link manipulator as pictured in Figure 3.1 can be thought of as a beam with torque applied at one end and free at the other end. There are several steps to determine the RHP zeros and imaginary poles of this system. First, develop a model for the beam. Second, determine the appropriate boundary conditions. Third, determine the system input and output. Forth, solve for the system zeros. The following sections will discuss each of these steps in more detail.
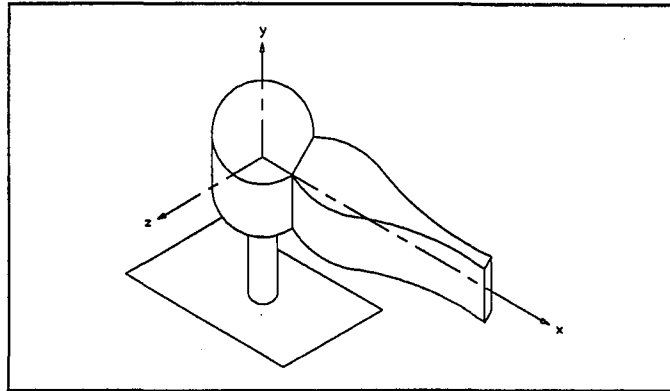
Figure 3.1: Single-Link, Flexible Manipulator

3.2.1 Element Approach to Modeling

A link with nonuniform cross-sections can be modeled as a series of discrete elements. While the shape of these elements is similar, the size can vary to allow for changes in cross-section. The appropriate element to model a flexible link is an Euler-Bernoulli beam element. The Euler-Bernoulli model neglects the effects of rotary inertia and shear deformation in the element.[12] This assumption is generally valid for modeling beams whose length is roughly ten times the height. Flexible manipulators have long, slender links which are appropriately modeled under the Euler-Bernoulli assumption.

Transfer matrices are derived from the equation of motion for a given element. For a uniform Euler-Bernoulli beam element, the equation of motion transformed to the frequency domain has the form:

$$\frac{d^4 w(x,\omega)}{dx^4} = \frac{\mu\omega^2}{EI} w(x,\omega) \qquad (3.2)$$

where,

$$
\begin{aligned}
\mu &= \text{mass density per unit length} \\
\omega &= \text{frequency in radians/second} \\
E &= \text{Young's modulus} \\
I &= \text{Cross sectional area moment of inertia}
\end{aligned}
$$

Notice the equation is fourth order thus requiring four states to describe the solution in transfer matrix form. The state vector for the Euler-Bernoulli element is:

$$u = \begin{bmatrix} -w \\ \psi \\ M \\ V \end{bmatrix} = \begin{bmatrix} displacement \\ slope \\ moment \\ shear\ force \end{bmatrix}$$

(3.3)

The first two elements of the state vector are displacements (w and ψ) while the last two elements are forces (V and M). This arrangement of states is characteristic of transfer matrix theory. Figure 3.2 shows how these are defined for transfer matrix theory.
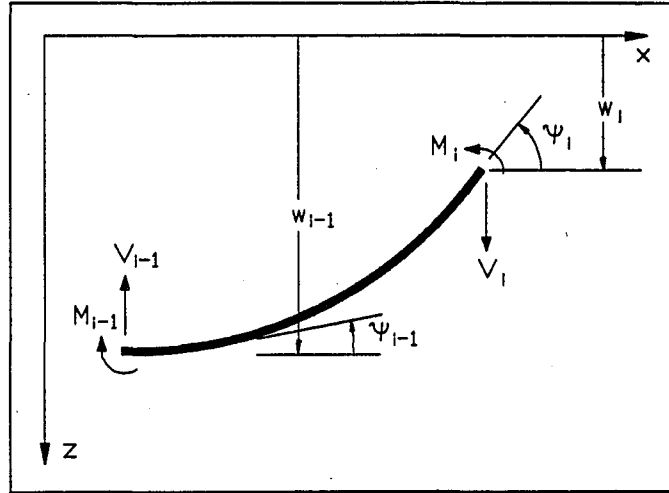

Figure 3.2: State Variables and Sign Conventions

An analytic solution to Eq. 3.2 can be found when the element has uniform properties (ie. constant cross-section, mass density, and stiffness). Eq. 3.4 gives the transfer matrix for a uniform Euler-Bernoulli element. Each element of Eq. 3.4 is a function of frequency and must be reevaluated as the frequency of interest changes.

$$TM = \begin{bmatrix} C_0 & lC_1 & aC_2 & alC_3 \\ \dfrac{\beta^4 C_3}{l} & C_0 & \dfrac{aC_1}{l} & aC_2 \\ \dfrac{\beta^4 C_2}{a} & \dfrac{\beta^4 lC_3}{a} & C_0 & lC_1 \\ \dfrac{\beta^4 C_1}{al} & \dfrac{\beta^4 C_2}{a} & \dfrac{\beta^4 C_3}{l} & C_0 \end{bmatrix}$$

(3.4)

where,

$$C_0 = \frac{1}{2}\left(cosh\,\beta + cos\,\beta\right)$$

(3.5)

$$C_1 = \frac{1}{2\beta}\left(sinh\,\beta + sin\,\beta\right)$$

$$(3.6)$$

$$C_2 = \frac{1}{2\beta^2}\left(cosh\,\beta - cos\,\beta\right)$$

$$(3.7)$$

$$C_3 = \frac{1}{2\beta^3}\left(sinh\,\beta - sin\,\beta\right)$$

$$(3.8)$$

and

$$\beta^4 = \frac{\omega^2\,l^4\,\mu}{E\,I}$$

$$(3.9)$$

$$a = \frac{l^2}{EI} \qquad (3.10)$$

With the transfer matrix for the fundamental beam elements, one can combine these elements serially to generate a model for the link. Figure 3.3 illustrates how a simple model can be constructed for a tapered beam. Although only two elements are considered here, more elements can be added to better approximate the shape of the link.
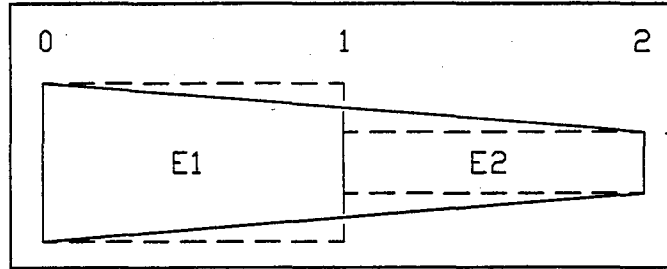

Figure 3.3: Simple Model of a Tapered Beam

Element E1 can be represented by the equation:

$$u_1 = [B_1]u_0 \qquad (3.11)$$

Similarly for element E2,

$$u_2 = [B_2]u_1 \qquad (3.12)$$

Since the states at interface u_1 are the same for both elements, u_1 can be eliminated to obtain an overall transfer matrix for the beam:

$$u_2 = [B_2][B_1]u_0 \qquad\qquad (3.13)$$

Eliminating one state simply illustrates the point that this multiplication can be carried out to eliminate all intermediate states in a model with more elements.

As previously mentioned, transfer matrices themselves are not numerical approximations. The transfer matrix for an Euler-Bernoulli beam contains the analytic solution for a uniform beam element. It is not an assumed modes solution. The approximation made in using transfer matrix theory involves the modeling of the beam and solution of the equations. To generate the model of a link with variable cross-section, the size of the elements must vary. The interface of two different size elements will be discontinuous. In Figure 3.3, interface 1 is discontinuous between elements E1 and E2. These discontinuities are the major approximation when using transfer matrices to model a beam. This approximation can be minimized by using more elements to model a nonuniform beam. As more elements are added to the model, the discontinuities between elements will decrease thus reducing the effects of this approximation on the results.

Transfer matrix theory is similar to Finite Element Analysis (FEA). In FEA, first the system must be discretized. Then an appropriate interpolation function must be selected to describe each element (i.e. element stiffness). Next the system matrices must be assembled to produce a set of linear algebraic equations. Finally the linear equations are solved to get an approximate solution to the system under consideration.

Like FEA, when using transfer matrices the system must be first discretized into a finite number of elements. Unlike FEA though, there is no approximate interpolation function needed to describe each element. Each matrix contains the analytic equations describing the element. The two methods also differ in the method of solution of the numerical system of equations (for this application). As will be explained later, a root finder is used to determine the location of poles and zeros. An equation is extracted from the overall transfer matrix based on the desired input and output and the boundary conditions. The root finder then searches this equation to determine the location of poles and zeros. Although both are numerical methods to find an approximate solution to a continuous system, transfer matrix theory does reduce some approximations by using exact solutions to the partial differential equations to describe the individual elements.

3.2.2 Boundary Conditions

The second step in finding the RHP zeros and imaginary poles of a system is applying the appropriate boundary conditions. As Figure 3.4 shows, there are several boundary conditions that can be applied to model a flexible link. The clamped-free condition corresponds to a rigid coordinate attached at the hub. The pinned-pinned condition corresponds to a rigid coordinate which passes through the end-point of the manipulator. In this research, the pinned-free boundary condition was chosen to model the flexible link. This corresponds to a rigid coordinate passing through the center of mass of the beam. This boundary condition was chosen because it naturally describes a flexible link and

because it allows easy comparison with previous research by Spector and Flashner[20,21] who also used these boundary conditions to model the flexible link.
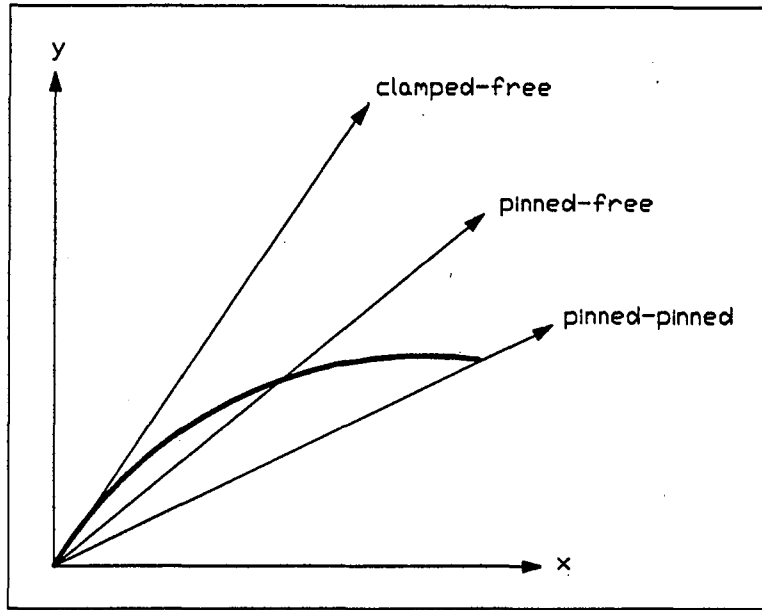

Figure 3.4: Boundary Conditions for a Flexible Link

A pinned-free boundary condition implies that:

At x=0 (base): $w=0$ $M=0$ (pinned)

At x=L (tip): $V=0$ $M=0$ (free)

These boundary conditions are applied to the overall transfer matrix for the system and the appropriate state variables are set to zero.

$$
\begin{bmatrix} -w \\ \psi \\ 0 \\ 0 \end{bmatrix}_{x=L} = \begin{bmatrix} B_{11} & \cdots & B_{14} \\ \vdots & \ddots & \vdots \\ B_{41} & \cdots & B_{44} \end{bmatrix} \begin{bmatrix} 0 \\ \psi \\ 0 \\ V \end{bmatrix}_{x=0}
$$

(3.14)

3.2.3 System Input and Output

When the system zeros are of interest, one must chose the system input and output. Unlike the natural frequency calculation which depends only on the boundary conditions, the location of system zeros will change as the input/output relationship changes. To illustrate this point, consider a single-link flexible manipulator modeled as a continuous system. Figure 3.5 shows the pole zero pattern of two different input/output relationships for the same system. Figure 3.5.a shows the transfer function between the joint angle, $\theta(s)$, and

joint torque, $\tau(s)$, to be minimum phase. This is expected since these two are collocated. Figure 3.5.b shows the transfer function between tip position, $X(s)$, and joint torque, $\tau(s)$, to be nonminimum phase. The RHP zeros are a result of the noncollocated output relationship. Since this research targets the location of RHP zeros the system output is tip position, and the system input is joint torque. Considering the system input and output, the overall system transfer matrix will have the form:
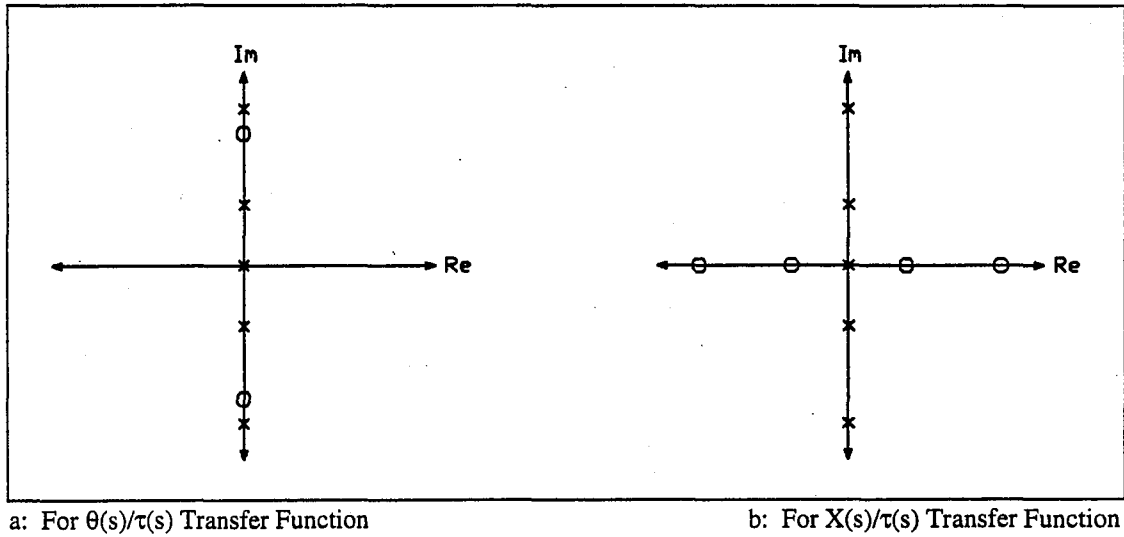

a: For $\theta(s)/\tau(s)$ Transfer Function   b: For $X(s)/\tau(s)$ Transfer Function

Figure 3.5: Pole/Zero Patterns For Different Input/Output Relationships

$$
\begin{bmatrix} -w \\ \psi \\ 0 \\ 0 \end{bmatrix}_{x=L} = \begin{bmatrix} B_{11} & \cdots & B_{14} \\ \vdots & \ddots & \vdots \\ B_{41} & \cdots & B_{44} \end{bmatrix} \begin{bmatrix} 0 \\ \psi \\ \tau \\ V \end{bmatrix}_{x=0}
$$

(3.15)

In the above equation, w_L is the system output which corresponds to tip position, and τ is the system input corresponding to joint torque at the base of the manipulator.

3.2.4 Zero Function

The zeros of a system are defined as the frequencies that result in zero system output for an arbitrary system input. To determine the system zeros, one must know a) the system input, b) the system output, and c) the relationship between the input and the output. This can be expressed in an equation of the form:

$$
INPUT = \left(\frac{TRANSFER}{FUNCTION} \right) * OUTPUT
$$

(3.16)

For an arbitrary input to the system, the only way to guarantee zero output is for the transfer function to be zero at the given frequency.

Given the boundary conditions chosen in Section 3.2.2 and the input/output relationship chosen in Section 3.2.3, Eq. 3.15 can be expanded to find the relationship between input and output. The four equations are:

$$-w_L = B_{12}\psi_0 + B_{13}\tau + B_{14}V_0 \qquad (3.17)$$

$$\psi_L = B_{22}\psi_0 + B_{23}\tau + B_{24}V_0 \qquad (3.18)$$

$$0 = B_{32}\psi_0 + B_{33}\tau + B_{34}V_0 \qquad (3.19)$$

$$0 = B_{42}\psi_0 + B_{43}\tau + B_{44}V_0 \qquad (3.20)$$

Since ψ_L is not of interest, Eqs. 3.17, 3.19, and 3.20 can be solved for the relationship between w_L and τ:

$$w_L = -\left[\frac{B_{12}B_{44}B_{33} - B_{12}B_{34}B_{43} + B_{13}B_{34}B_{42} - B_{13}B_{44}B_{32} + B_{14}B_{43}B_{32} - B_{14}B_{33}B_{42}}{B_{34}B_{42} - B_{44}B_{32}} \right]\tau$$

$$(3.21)$$

Where the B_{ij} are elements of the overall transfer matrix in Eq. 3.15. When the function inside the brackets is zero (for a given frequency), the output will always be zero regardless of the input; therefore, the zeros of the bracketed term are the system zeros.

$$f(\omega) = \left[\frac{B_{12}B_{44}B_{33} - B_{12}B_{34}B_{43} + B_{13}B_{34}B_{42} - B_{13}B_{44}B_{32} + B_{14}B_{43}B_{32} - B_{14}B_{33}B_{42}}{B_{34}B_{42} - B_{44}B_{32}} \right]$$

$$(3.22)$$

To search for RHP zeros, one must consider what type of frequency to input into Eq. 3.22. Using the relationship which defines the Laplace variable, s

$$s = j\omega \qquad (3.23)$$

one can easily determine ω should have the form:

$$\omega = 0 - jb \qquad \text{where } 0 \le b \le \infty \qquad (3.24)$$

Purely imaginary negative values of ω will result in purely real positive values of s. Thus searching Eq. 3.22 with frequencies of the form of Eq. 3.24 one can find the location of the RHP zeros. Assuming the damping factor to be zero, it can be shown that the elements of the transfer matrix are real for a purely complex frequency. If the elements of the transfer matrix are real, the zeros function, Eq. 3.22, will also be real.

3.2.5 Natural Frequency Function

Although the location of RHP zeros is of primary concern in this research, knowledge of pole location will help in analysis of the results. Since the system damping is ignored, the poles will lie on the imaginary axis of the s-plane in complex conjugate pairs. The location of these poles can be determined by simply searching the positive imaginary axis of the s-plane. Considering the applied boundary conditions, one can extract two homogeneous equations from Eq. 3.14 to get the homogeneous system:

$$\begin{Bmatrix} 0 \\ 0 \end{Bmatrix} = \begin{bmatrix} B_{32} & B_{34} \\ B_{42} & B_{44} \end{bmatrix} \begin{Bmatrix} \psi \\ V \end{Bmatrix} \tag{3.25}$$

The poles (eigenvalues) of the system are those values of ω which make the determinant of the sub-transfer matrix in Eq. 3.25 equal to zero (see Book, et al.[6] for a detailed explanation). For a two by two matrix this determinant is simply:

$$g(\omega) = B_{32} B_{44} - B_{34} B_{42} \tag{3.26}$$

Referring to Eq. 3.23, one finds that Eq. 3.26 is the denominator of the input/output transfer function which is to be expected. To find the values of the purely complex poles, one must search Eq. 3.26 for its roots. According to the definition of s, ω must have the form:

$$\omega = b + j0 \tag{3.27}$$

Searching over a range of values for b will give the poles in that range. With the zero and natural frequency functions determined, the problem remains to implement a computer solution to find the RHP zeros and imaginary poles.

3.2.6 Mode Shapes For Pinned-Pinned Boundary Condition

To implement the results of this research in the inverse dynamic control algorithm developed by Kwon and Book[9], the mode shapes must be determined for pinned-pinned boundary conditions. The natural frequencies for a tapered link are easily determined with the tapered link algorithm. Pinned-pinned boundary conditions change the frequency determinant which changes the search function.

The tapered design was chosen so that A=0.6 in. and B=0.3 in. (R=2.0). As described earlier, the beam has L=40 in., H=1 in., and properties of aluminum. For a discussion of mode shape generation using transfer matrices see Majette[11].

The state matrix consists of the state vectors at each interface for the given natural frequency. The chosen design has twenty elements; therefore, the state matrix will have twenty-one columns and four rows. Recall from Section 3 that the state vector is described by Eq. 3.3. Figures 3.6 and 3.7 present the mode shapes for the first and second natural frequencies respectively.

3.3 Computer Algorithm

Like Finite Element Analysis, the solution to pole/zero location of a flexible link using transfer matrix theory is computationally intensive. As the number of elements in the model increases, so does the number of computations. With the availability of computers today, the problem is fairly easy to solve if the proper algorithm can be implemented. Previous research by Book and others[6,11] used transfer matrices to model systems and this provided some insight on how to realize a computer solution using transfer matrices, especially the DSAP[6] package. The program structures are purposely similar to aid in combining the programs for future research.
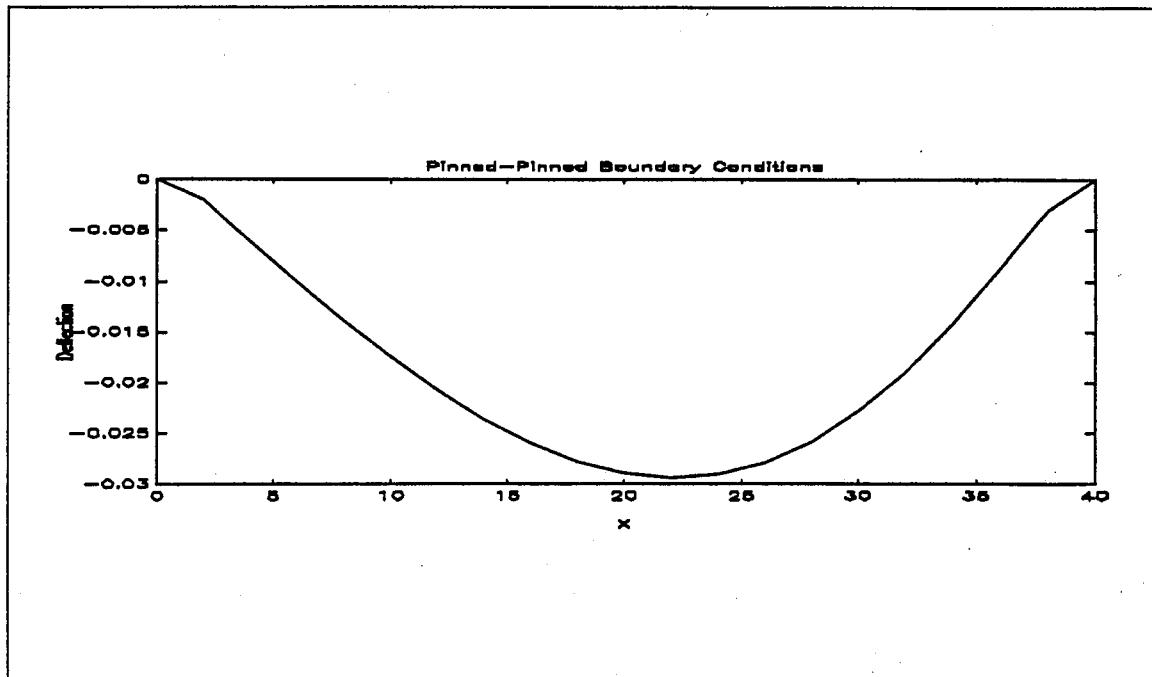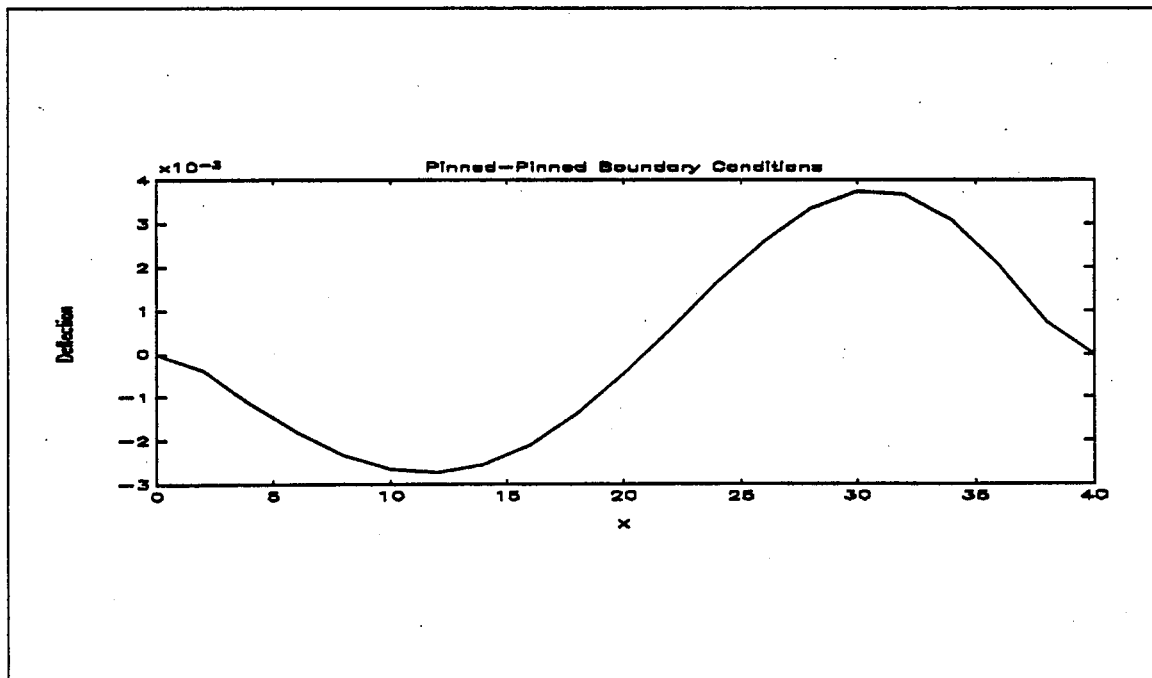
Figure 3.6: First Mode Shape For Tapered Link

Figure 3.7: Second Mode Shape For Tapered Link

4. Results

The results of the zero and pole locations found from the Transfer Matrix approach are presented in this section as a collection of examples. Each example investigates a different aspect of the relationship between RHP zero location and structural link design. As previously noted, pole location is often of interest to the designer; therefore, this information is presented for each example. Unless otherwise specified, several dimensions remain the same from one example to the next (referred to as nominal dimensions). The overall length of the beams is 40 inches, and the height (which remains constant over length) is 1 inch. The material properties are selected to be those of aluminum: modulus of elasticity, E, is 10E6 psi, and the density is 9.55E-2 lb/in^3.

4.1 Validity of Results

$$\omega_n = (\beta_n l)^2 \left(\frac{EI}{\rho A l^4} \right)^{\frac{1}{2}} \tag{4.1}$$

Before examining the relationship between RHP zeros and link design, the validity of the computer algorithm to determine zero/pole location must first be checked. Since analytic solutions exist for the location of poles for a uniform beam, the results from the Transfer Matrix approach are compared to the analytic solution to determine the accuracy of the algorithm. The vibrations text by Rao[19] contains the analytic solution for pole location of a pinned-free beam under lateral vibration. The poles are determined from the following equation:

For a pinned-free beam, the values of $\beta_n l$ are:

$$\beta_1 l = 3.926602$$
$$\beta_2 l = 7.068583$$
$$\beta_3 l = 10.210176$$

For a uniform beam with width=0.5 inches and nominal properties as given above, the pole locations are presented in Table 4.1 along with the results from the Transfer Matrix approach.

Table 4.1: the Transfer Matrix vs. Analytical Solution

Pole	Transfer Matrix	Analytical Solution
1	14.23	14.23
2	46.12	46.12
3	96.23	96.23

The results generated from the Transfer Matrix approach show excellent correspondence to the analytic values. However analytic calculation of zeros is not as simple of a task since the boundary conditions are no longer homogeneous, and texts lack tabulated results

It must be noted that the results presented in this section will not include the two poles lying at the origin. These poles are a result of the rigid body mode of the system. Keep in mind the location of the poles will be presented as a real number, but they actually are located on the s-plane in complex conjugate pairs along the imaginary axis. The zeros are also presented as real numbers, and they lie on the real axis as reflected pairs about the imaginary axis. This means for every RHP zero, there is a corresponding LHP zero equal in magnitude but opposite in sign. The symmetry of the s-plane results from ignoring the damping of the structure in the Euler-Bernoulli model and is confirmed by Spector and Flashner[20].

4.2   Effects of Discretization

When modeling a continuous system with a discrete model, one should check to make sure the discretization of the model does not affect the results. This is easily confirmed by studying a uniform beam. Using transfer matrices, a uniform beam can be modeled with one element or several elements. It has been cofirmed in earlier publications that this has no effect.[8] For a tapered beam, the number of elements will be more critical because increasing the elements will decrease the discontinuities at each element interface. This should result in a better approximation of the tapered link. For nonuniform designs, the poles and zeros should converge to the actual values as the number of elements increases. This will be confirmed later in this section.

4.3   Modeling of a Tapered Beam

Another point to consider in the computer implementation of the RHP zeros problem is how well does the model represent the actual system. Although the model is limited to uniform elements, there are any number of combinations one can find to represent the system. This example examines two different methods for modeling a linearly tapered beam. As shown in Figure 4.1 the link is tapered along the length in the width dimension while the height was held constant. The taper is described by two dimensions: the width at the base, A, and the width at the tip, B. The degree of taper, R=A/B, is used to compare different designs.
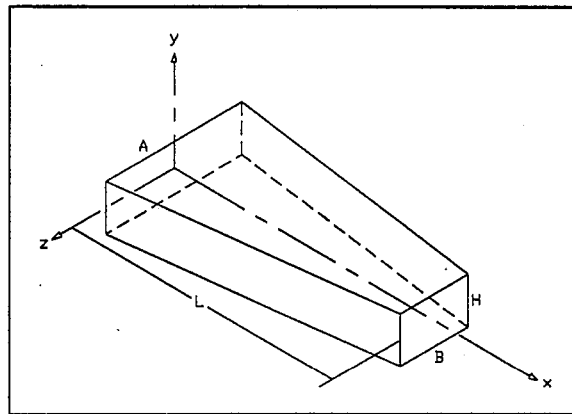

Figure 4.1: Tapered Link Diagram

Using Method 1 to model the tapered link, the beam is divided into elements of equal length. For a three element model with length L, each element will have length L/3. The height of each element is the same, while the width of each element changes linearly as a function of x. Figure 4.2 presents Method 1.
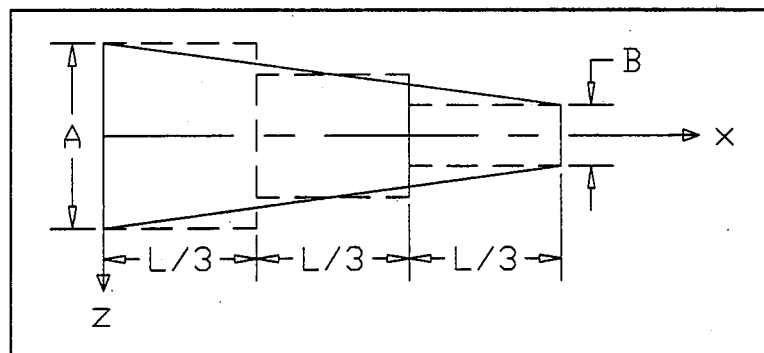

Figure 4.2: Modeling Method 1

Using Method 2 to model the tapered link, the beam is divided into elements so the first and last element have length one-half of the intermediate elements. For a three element

model with length L, the first and last elements will have length L/4 and the middle element will have length L/2. Again the height of each element ss the same, while the width of each element changes linearly as a function of x. Figure 4.3 presents Method 2.
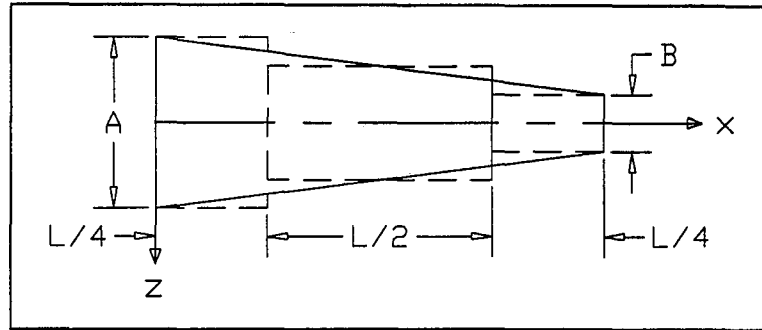

Figure 4.3: Modeling Method 2

Figures 4.2 and 4.3 illustrate the main difference between the two modeling methods. Method 2 compensates the elements at each end for meeting the specified end widths A and B. In both methods the width of intermediate elements is determined by the width of the tapered beam at the midpoint of each element. Since the end elements meet the specified A and B, the tapered link will not pass through the midpoint of these two elements. Method 2 compensates for this exception by making the end element lengths one half the length of the other elements.

To compare these two different methods for a linearly tapered beam, a beam with nominal dimensions and A=0.75 inches and B=0.25 inches is examined. This corresponds to R=3. The number of elements is increased with each method until the zeros and poles converge. Figure 4.4 presents the results from Method 1 where all elements are of equal length, and Figure 4.5 presents the results from Method 2 where the end elements are half the length of all other elements. Although only two methods are considered in this research, there are many different ways to discretize a nonuniform link.

The two methods are evaluated based on an error function. When the tapered beam is modeled with 80 elements, both methods converge to nearly identical values for the poles and zeros. These values, when NE=80, are taken to be the "correct' values and other cases are compared to this case. The error, e, is defined for the zeros as:

$$e = \left| \frac{z_{80,i} - z_{NE,i}}{z_{80,i}} \right|$$

(4.2)

where i refers to the ith zero

A similar definition is used for the poles. As the figures show, Method 2 provides better results for the same number of elements. For a targeted error of less than 1%, Method 2 reaches the target with NE=10 while Method 1 requires NE=20 to reach the target. Thus,

compensating the end elements does provide a better model of a linearly tapered beam, and this method is used in the following examples unless specified otherwise
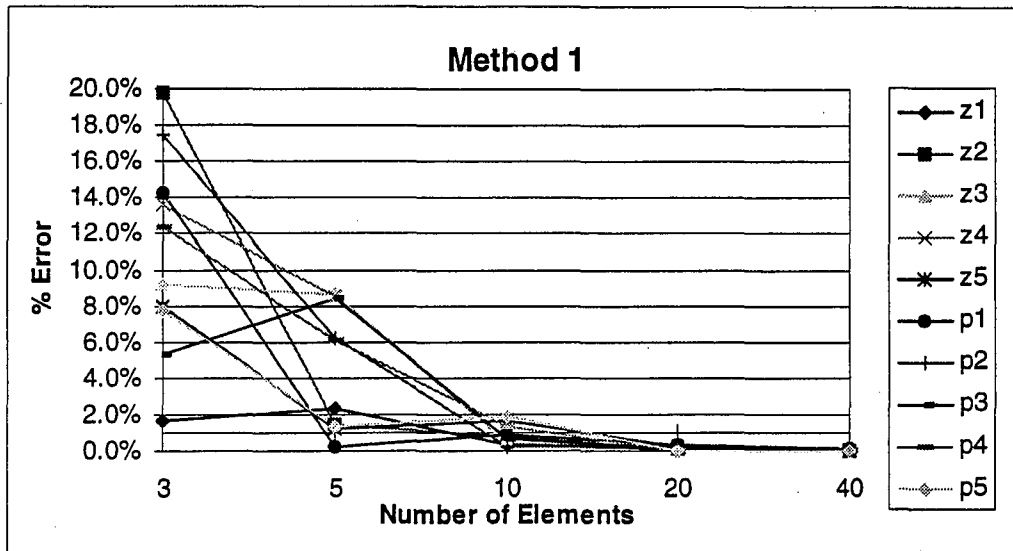

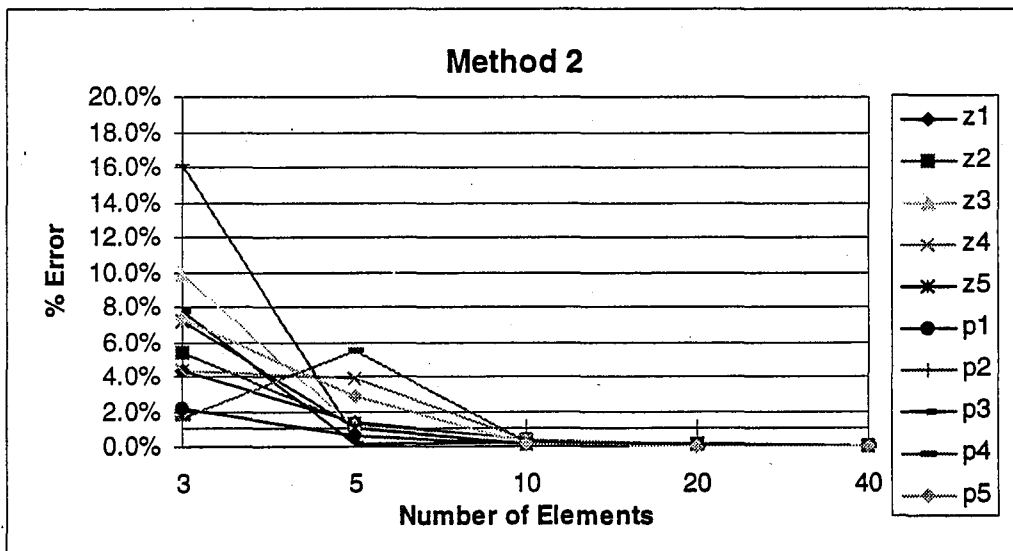Figure 4.4: Percentage Error for Method 1 for Poles (p1...p5) and Zeros (z1...z5)

Figure 4.5: Percentage Error for Method 2 for Poles (p1...p5) and Zeros (z1...z5)

4.4 Linear Taper Designs

When comparing different link designs to evaluate pole/zero location as a function of link shape, it is necessary to keep some parameters constant to aid in the evaluation. For a

single-link manipulator rotating in the horizontal plane, the link's mass moment of inertia about its axis of rotation, I_y, is of importance. This parameter directly affects the dynamic equations of motion and is an important design parameter in terms of motor selection. In the following studies, several link designs are evaluated for a given value of I_y. A tapered link's moment of inertia about its axis of rotation in terms of the links parameters: L, A, B, H, and ρ is given by the following equation:

$$I_y = \frac{\rho H}{48}(A^3 + A^2 B + AB^2 + B^3 + 4AL^2 + 12BL^2)$$

(4.3)

For a given tapered link design, one can use Eq. 4.3 to determine I_y. Knowing I_y, one can change the value of A and solve Eq. 4.3 for B. Since the equation is cubic in B, a commercial package like *Mathematica* can be used to solve for B. Following this method, a group of tapered link designs are generated for given values of I_y. Figures 4.6 shows pole/zero maps for selected values of R for I_y=764.05.

Several patterns are evident by examining the graph. First as a general rule, both the poles and zeros increase (move away from the origin) as the taper on the beam is increased. Increasing the taper effectively moves more of the link's mass closer to the base. Increasing the magnitude of the poles is often desirable to push them out of the system bandwidth and increase system response time. The ordering of poles and zeros is the second pattern recognized. In a minimum phase system, the poles and zeros will both lie on the imaginary axis in complex conjugate pairs and in an alternating order. This means, along the imaginary axis, the poles and zero are found in the order p_1,z_1,p_2,z_2, etc. or vice versa. Previous research[20] has found this alternating order of poles and zeros does not hold for nonminimum phase systems. It is not obvious in Figure 4.6, but the pole/zero order does not alternate. The actual order is: $z_1,p_1,p_2,z_2,p_3,z_3,p_4,p_5,z_4$.... p_2 jumps in front of z_2, and the same occurs for p_5. This reordering of poles and zeros can be critical as accurate knowledge of the pole/zero order is important for control system design.
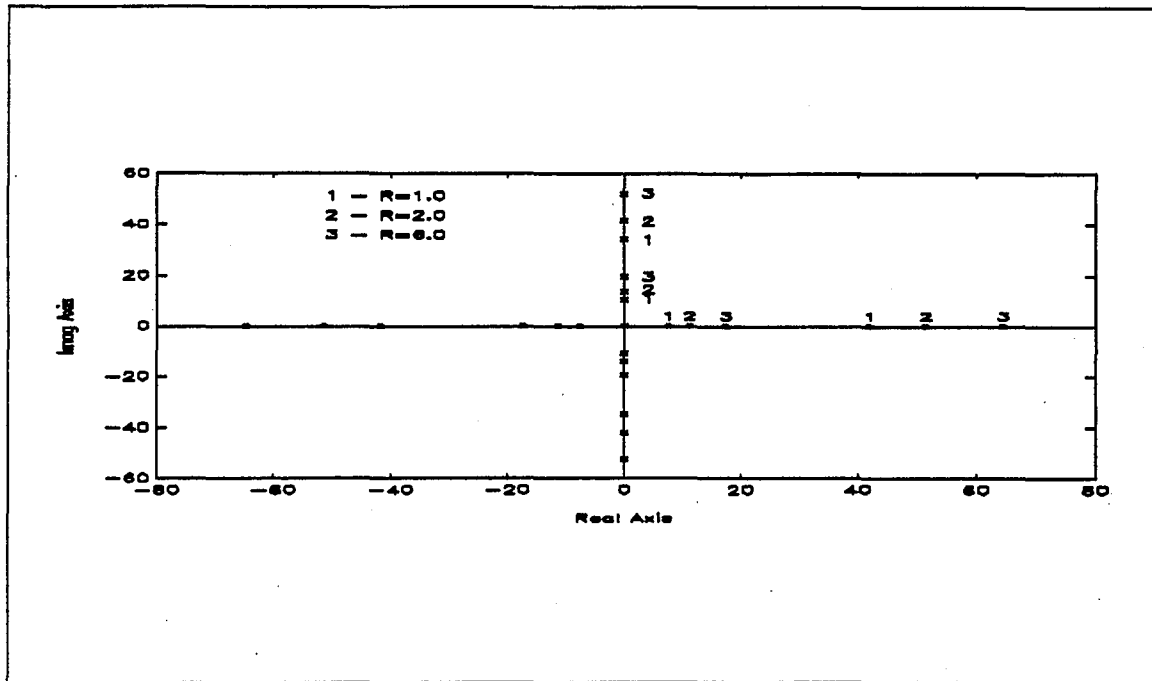
Figure 4.6: Pole/Zero Map of Selected Designs For I_y=764.05

4.4.1 Designs With Constant I_y

Important information is learned from examining the relationship between the taper ratio, R, and the values of the normalized zeros. The first normalized zero is of most importance. Figure 4.7 shows this relationship for data with Iy=764.05 and Iy=1528.1. Both curves are fitted with a third order polynomial. Even though the coefficients are different for each polynomial fit, the curves are nearly identical.

This illustrates an important relationship in the design of tapered links. For a given ratio R, the normalized zero will always remain the same. The designer can choose the location of the first pole and zero, determine the normalized zero, and then using Figure 4.8 find the appropriate taper ratio R. Of course there are constraints on this process. A ratio less than one corresponds to a taper with B greater than A, which is usually undesirable. At the other end, R is limited by the value of H. If A is larger than the value of H, the link will be wider at the base than it is tall, and the assumption that the link is stiff in the vertical plane will no longer be valid. Although the designer can choose the pole/zero relationship, the values of normalized zeros are limited to approximately 0.72-0.82 (according to Figure 4.7).
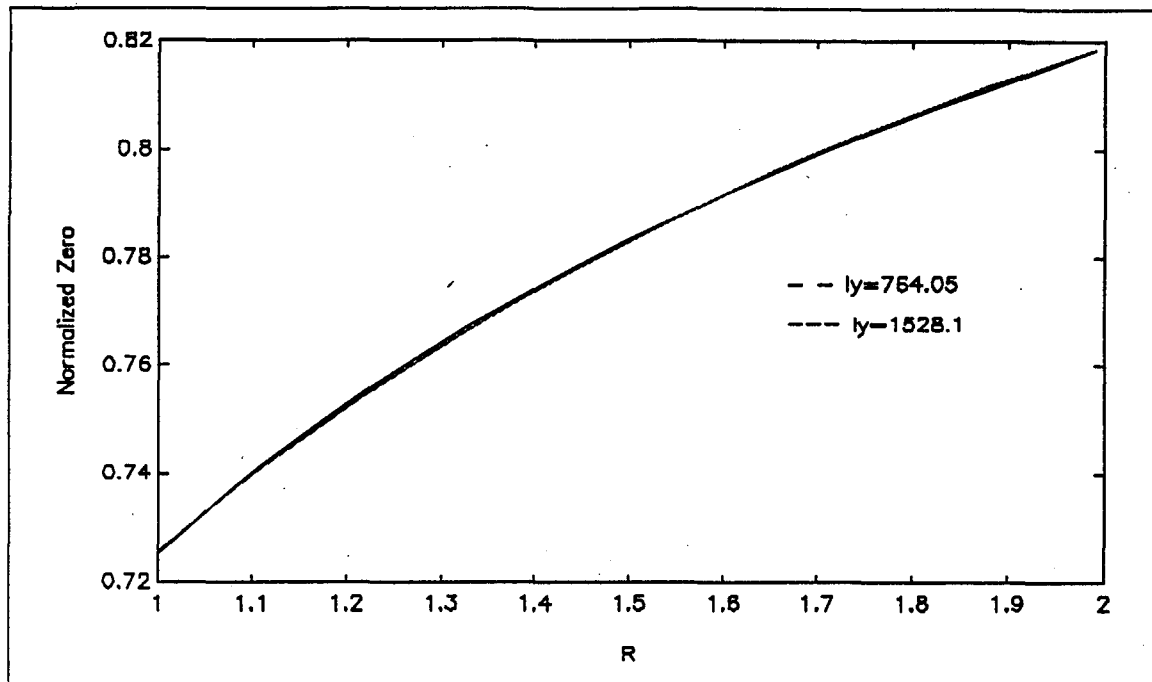
Figure 4.7: Comparison of Polynomial Curve Fits

4.4.2 Designs With Constant Poles and Zeros

The previous example demonstrates how the designer can choose the pole/zero relationship and then determine the appropriate taper design. Once the taper is chosen, the designer can change the link height to independently adjust the value of I_y. Since the adjustment of H is out of the plane of motion, it has no effect on the location of poles and zeros. Combining this with the results from the previous example, the designer can effectively choose the location of poles and zeros and independently adjust the links moment of inertia about its axis of rotation to meet the needs of the particular system.

5. Conclusions

This algorithm is developed as a tool to locate the poles and zeros of a single-link manipulator modeled as a pinned-free Euler-Bernoulli beam. The algorithm uses transfer matrix theory to allow for variable cross-sections granting the designer new freedom in analysis of nonuniform link designs. The results are shown to be very accurate when system pole location is compared to analytic solutions for uniform beams. Several results from previous research are confirmed.

First, the reordering of poles and zeros is confirmed for nonminimum phase systems. Accurate knowledge of pole/zero order is critical for proper control system design. Even with very few elements in the model, this algorithm predicts the proper order of poles and zeros.

Second, the examples presented suggest the nonminimum phase characteristics can not be eliminated by changing the structural design of the link. The system will be nonminimum phase above a finite frequency dictated by the location of the first nonminimum phase zero. It is possible that this frequency is out of the operating range and not of concern to the designer.

This algorithm is set up specifically for pinned-free boundary conditions of the model and determines pole and zero location based on a user determined frequency range. Linearly tapered beams have been presented in this chapter, but any type of nonuniform beam can be analyzed with this method. Slight modifications would also allow for different boundary conditions.

The design procedure for tapered beams allows the designer to choose the first pole and zero subject to certain physical constraints. These physical constraints only allow for approximately 25% variation in R. This zero to pole ratio defines a particular taper ratio according to the collected data. Keeping the ratio the same, the size of the taper can be changed to get the proper magnitude of the pole and zero. With the pole and zero placed, the height of the beam can be changed to adjust the link's moment of inertia about its axis of rotation. This procedure can be used to design tapered links to meet the particular requirements of the system.

The material presented is for a single-link manipulator modeled with pinned-free boundary conditions. This is a simplified model, but it is necessary to show transfer matrices yield good results for this case before progressing to more complicated problems. Now that transfer matrices have proven useful to solve for zero location, future work exists to extend these results.

First, a program could be developed so the user could input the desired boundary conditions which best represent the system. This could include hub inertia or end-point mass. Second, the program could be extended to multi-link designs to predict pole and zero location for different configurations. Transfer matrices have been derived for rotary joints and many other elements. The DSAP package developed by Book, et. al.[6] handles multi-link models and would be a good reference. Finally, the results for tapered link designs could be applied to the inverse dynamic algorithm developed by Kwon and Book[10]. This method requires mode shapes for the assumed modes and uses pinned-pinned boundary conditions as presented in Section 3.2.6.

REFERENCES

1   Asada, H., Park, J.-H., and Rai, S., "*A Control-Configured Flexible Arm: Integrated Structure/Control Design,*" **Proceedings of the 1991 IEEE International Conference on Robotics and Automation**, Sacramento, California, April, 1991, pp. 2356-2362.

2   Bayo, E., "*A Finite Element Approach to Control the End-Point Motion of a Single-Link Flexible Robot,*" **Journal of Robotic Systems**, Vol. 4, No. 1, 1987, pp.63-75.

3   Beer, Ferdinand, and Johnson, Russell, Jr., *Vector Mechanics for Engineers, Statics and Dynamics*, Third Edition, McGraw-Hill, New York, 1977.

4   Book, W. J., *Design and Control of Flexible Manipulator Arms*, Ph.D. Thesis, Massachusetts Institute of Technology, April, 1974.

5   Book, W. J., and Kwon, D.-S., "*Contact Control for Advanced Applications of Light Weight Arms,*" **Symposium on Control of Robots and Manufacturing**, Arlington, Texas, 1990.

6   Book, W. J., Majette, M., and Ma, K., *The Distributed Systems Analysis Package (DSAP) and Its Application to Modeling Flexible Manipulators*, NASA Contract NAS 9-13809, Subcontract No. 551, School of Mechanical Engineering, Georgia Institute of Technology, 1979.

7   Churchill, R. V., and Brown, J. W., *Complex Variables and Applications*, Fifth Edition, McGraw-Hill Publishing Company, New York, 1990.

8   Girvin, D.L. *Numerical Analysis of Right-Half Plane Zeros for a Single-Link Manipulator*, Master's Thesis, Georgia Institute of Technology, Mechanical Engineering, March, 1992.

9   Kwon, D.-S., *An Inverse Dynamic Tracking Control for Bracing A Flexible Manipulator*, Ph.D. Dissertation, Georgia Institute of Technology, Mechanical Engineering, June, 1991.

10   Kwon, D.-S., and Book, W. J., "*An Inverse Dynamics Method Yielding Flexible Manipulator State Trajectories,*" **Proceedings of the American Control Conference**, June, 1990, pp. 186-193.

11   Majette, M., *Modal State Variable Control of a Linear Distributed Mechanical System Modeled with the Transfer Matrix Method*, Master's Thesis, Georgia Institute of Technology, Mechanical Engineering, June, 1985.

12   Meirovitch, L., *Elements of Vibrational Analysis*, McGraw-Hill, New York, 1986.

13   Misra, Pradee, "*On The Control of Non-Minimum Phase Systems,*" **Proceedings of the 1989 American Control Conference**, 1989, pp. 1295-1296.

14   Miu, D.K., "*Physical Interpretation of Transfer Function Zeros for Simple Control Systems with Mechanical Flexibilities,*" **Journal of Dynamic Systems, Measurement, and Control**, Vol. 113, September, 1991, pp. 419-424.

15   Nebot, E. M., Lee, G. K. F., and Brubaker, T. A., "*Experiments on a Single Link Flexible Manipulator,*", **Proceedings from the USA-Japan Symposium on**

Flexible Automation Crossing Bridges: Advances in Flexible Automation and Robotics, 1988, pp. 391-398.

16   Park, J.-H., and Asada, H., *"Design and Analysis of Flexible Arms for Minimum-Phase Endpoint Control,"* **Proceedings of the American Control Conference,** 1990, pp. 1220-1225.

17   Park, J.-H., and Asada, H., *"Design and Control of Minimum-Phase Flexible Arms with Torque Transmission Mechanisms,"* **Proceedings   of the 1990 IEEE International Conference on Robotics and Automation,** 1990, pp. 1790-1795.

18   Pestel and Leckie, *Matrix Methods in Elastomechanics,* McGraw-Hill, New York, 1963.

19   Rao, Singiresu S., *Mechanical Vibrations,* Addison-Wesley Publishing Company, Reading, Massachusetts, 1986.

20   Spector, V. A., and Flashner, H., *"Modeling and Design Implications of Noncollocated Control in Flexible Systems,"* **Journal of Dynamic Systems, Measurement, and Control,** Vol. 112, June, 1990, pp. 186-193.

21   Spector, V. A., and Flashner, H., *"Sensitivity of Structural Models for Noncollocated Control Systems,"* **Journal of Dynamic Systems, Measurement, and Control,** Vol. 111, December, 1989, pp. 646-655.